J Mater Sci: Mater Electron (2018) 29:524–534
DOI 10.1007/s10854-017-7943-x

Enhanced electrochemical properties of $Li[Li_{0.2}Mn_{0.54}Ni_{0.13}Co_{0.13}]O_2$ with ZrF_4 surface modification as cathode for Li-ion batteries

Yuxiang Zuo[1,2] · Bing Huang[1,2] · Changmei Jiao[1,2] · Rongguan Lv[1,2] · Guangchuan Liang[1]

Received: 31 July 2017 / Accepted: 30 September 2017 / Published online: 10 October 2017

Abstract The amorphous ZrF_4 layer with various concentrations coated $Li[Li_{0.2}Mn_{0.54}Ni_{0.13}Co_{0.13}]O_2$ cathodes were synthesized by using the chemical deposition technology. The combinations of XRD, SEM and TEM results indicated that the nanoparticles ZrF_4 layer was successfully covered on the surface of the $Li[Li_{0.2}Mn_{0.54}Ni_{0.13}Co_{0.13}]O_2$ particles. Compared to the pristine $Li[Li_{0.2}Mn_{0.54}Ni_{0.13}Co_{0.13}]O_2$, the cathodes after ZrF_4 coating demonstrated the obviously enhanced electrochemical properties. The 2 wt% ZrF_4-coated $Li[Li_{0.2}Mn_{0.54}Ni_{0.13}Co_{0.13}]O_2$ delivered a high capacity retention of 91.9% after 100 cycles at 0.5 C, much higher than that (84.5%) of the uncoated sample. Besides, the discharge capacity of 2 wt% ZrF_4-coated $Li[Li_{0.2}Mn_{0.54}Ni_{0.13}Co_{0.13}]O_2$ was approximately 20.0 mAh g^{-1} larger than that of the pristine $Li_{1.20}[Mn_{0.54}Ni_{0.13}Co_{0.13}]O_2$ at various current densities. The EIS analysis indicated the remarkably enhanced electrochemical properties of the surface-modified electrode was ascribed to the fact that the ZrF_4 coating layer could restrict the side reaction between cathodes with electrolyte and protect the cathode surface from HF corrosion, further accelerate the Li^+ diffusion rate in the cathode.

✉ Guangchuan Liang
GuangchuanLiang@foxmail.com

[1] Institute of Power Source and Ecomaterials Science, Key Laboratory For New Type of Functional Materials in Hebei Province, Hebei University of Technology, Tianjin 300130, China

[2] School of Chemistry and Chemical Engineering, Yancheng Teachers University, Yancheng 224051, China

1 Introduction

Among all energy storage devices, Li-ion batteries (LIBs) have been widely used in electronic products, military and our daily life, owing to their obvious advantages including reliable stability, environmental protection and long lifespan [1–3]. However, with the fast development of electric automobile and large-scale energy-storage systems, the traditional cathode materials, such as layered $LiCoO_2$ and $LiMn_{1/3}Ni_{1/3}Co_{1/3}O_2$, olivine $LiFePO_4$ and spinel $LiMn_2O_4$, cannot satisfy the demands of the energy density [4–7]. Recently, the Li-excess $xLi_2MnO_3{\cdot}(1–x)LiMO_2$ (M = Mn, Ni, Co, etc.) materials, composed of the trigonal $LiMO_2$ (M = Ni, Co, and Mn) phase and the monoclinic Li_2MnO_3 phase, have attracted much study as cathode for LIBs when applied to the high power output equipment owing to the high theoretical specific capacity (> 250 mAh g^{-1}) and the high operating potentials (> 4.5 V) [8, 9].

However, with the further study on the $xLi_2MnO_3{\cdot}(1–x)LiMO_2$ materials, people have discovered that the high working voltage will cause some drawbacks, such as severe capacity degradation and poor thermal stability [10, 11]. To resolve the intrinsic defects, much effort has been made to enhance the electrochemical properties. Thereinto, the surface coating modification have demonstrated the obvious effects to improve the electrochemical properties for that the coating layer can effectively protect the cathode from reacting with the electrolyte and retard the thickening of SEI film [12–15]. Through literature, ZrO_2 has the highest fracture toughness, and can form a fracture-toughened thin-film solid solution near the particle surface. This film will significantly improve the structural stability of the cathode material by suppressing phase transition of cathode, thereby preventing capacity fading during electrochemical cycling [16, 17]. For example, when the ultrathin ZrO_2 coatings were

adopted to modify the surface of $LiNi_{0.5}Co_{0.2}Mn_{0.3}O_2$ cathode material by using the atomic layer deposition method, the 5-ZrO_2 coated sample maintained a high capacity retention of 96.2%, much larger than that (86.4%) of the bare sample [18]. Besides, the confined ZrO_2 encapsulation over high capacity spinel-layer-layer structured $0.5Li[Ni_{0.5}Mn_{1.5}]O_4{\cdot}0.5[Li_2MnO_3{\cdot}Li(Mn_{0.5}Ni_{0.5})O_2]$ with various concentration were synthesized by sol–gel method. And the 1 wt% ZrO_2 modification sample delivered the better cycle-ability, rate capability and high temperature performance than those of the bare cathode [17]. Therefore, ZrO_2 has been tested to be the effective surface modification material to improve the electrochemical properties of cathode materials. However, the hydrolysis of electrolyte with a trace amount of water can form the HF, and the oxide coating materials are unstable in HF environment. While the ZrF_4 can resist the HF acid etching and demonstrate the chemical stable under the environment of HF [19], therefore ZrF_4 maybe an attractive material to coat on the surface of the Li-excess $xLi_2MnO_3{\cdot}(1–x)LiMO_2$ cathode.

In the work, the ZrF_4 nanoparticles of various concentration were proposed to coated on the surface of $Li[Li_{0.2}Mn_{0.54}Ni_{0.13}Co_{0.13}]O_2$ cathode via using simple chemical deposition method to expectedly maintain the electrochemical properties stability. The influences of the ZrF_4 surface modification on the microstructure, morphology and electrochemical properties of $Li[Li_{0.2}Mn_{0.54}Ni_{0.13}Co_{0.13}]O_2$ cathode have been investigated deeply.

2 Experimental section

The pristine Li-excess $Li[Li_{0.2}Mn_{0.54}Ni_{0.13}Co_{0.13}]O_2$ was synthesized via using the carbonate co-precipitation method, followed by the high-temperature solid state reaction between $[Mn_{0.54}Ni_{0.13}Co_{0.13}](CO_3)_{0.8}$ precursors with $LiOH{\cdot}H_2O$. Firstly, the aqueous solution containing $MnSO_4{\cdot}H_2O$, $NiSO_4{\cdot}6H_2O$, and $CoSO_4{\cdot}7H_2O$ with the molar ratio of 0.54:0.13:0.13 was pumped into a continuous stirred reactor filled with nitrogen. Meanwhile, the appropriate amount of chelating agent ($NH_3{\cdot}H_2O$) and precipitant (Na_2CO_3) were added to the above reactor container to adjust the pH of the solution between 8.0 and 8.5. Then the whole solution in the water bath of 60 °C was continually stirred until the $[Mn_{0.54}Ni_{0.13}Co_{0.13}](CO_3)_{0.8}$ precursors have been acquired. Finally, the stoichiometric amount of $[Mn_{0.54}Ni_{0.13}Co_{0.13}](CO_3)_{0.8}$ precursors and the moderate amount of $LiOH{\cdot}H_2O$ powders have been grind uniformly and pre-heated at 500 °C for 7 h, followed by sintered at 950 °C for 12 h in tube furnace to obtain the pristine $Li[Li_{0.2}Mn_{0.54}Ni_{0.13}Co_{0.13}]O_2$ cathode materials [9, 19].

To prepare the ZrF_4 coated $Li[Li_{0.2}Mn_{0.54}Ni_{0.13}Co_{0.13}]O_2$ samples with the coating contents of 1, 2, and 3 wt%, respectively, the simple chemical deposition method was adopted as shown in Fig. 1. Firstly, the stoichiometric amount of pristine $Li[Li_{0.2}Mn_{0.54}Ni_{0.13}Co_{0.13}]O_2$ powers were immersed into the mixed solution, containing the $Zr(NO_3)_4$ and NH_4F with the corresponding molar ratio of 1:4. Then the above suspension solution has been under the water bath treatment at 85 °C with the continually stirring until the solvent has been evaporated completely. Finally, the obtained powers was calcined at 450 °C for 4 h in air to get the target samples, i.e. 1, 2 and 3 wt% ZrF_4-coated $Li[Li_{0.2}Mn_{0.54}Ni_{0.13}Co_{0.13}]O_2$.

To investigate the influence of the ZrF_4 coating layer on the crystal structure of $Li[Li_{0.2}Mn_{0.54}Ni_{0.13}Co_{0.13}]O_2$, the XRD measurements were carried out by using Rigaku RINT2400 X-ray diffractometer with Cu Kα radiation in the $10° \le 2\theta \le 80°$. The morphologies of synthesized materials were observed by using scanning electron microscopy (FE-SEM, JSM-7001F, JEOL). And the transmission electron microscope (TEM, JEOL JEM 2010) was adopted to examine the coating layer of cathode particles, coupled with an energy dispersive spectrum X-ray detector (EDS) to analyze the element composition.

The cathodes were prepared by mixing the above materials with carbon black and poly (vinylidene fluoride) (PVDF) binder at the weight percentage of 80, 10, and 10 wt%,

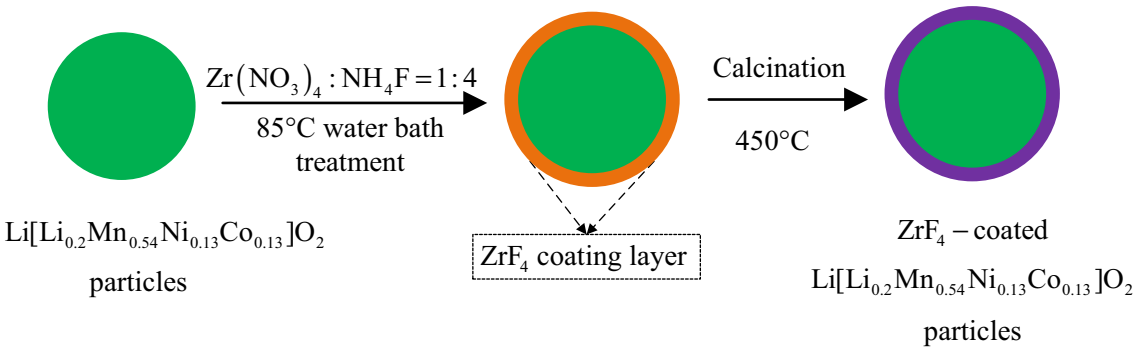

Fig. 1 Synthesis of ZrF4-coated $Li[Li_{0.2}Mn_{0.54}Ni_{0.13}Co_{0.13}]O_2$ samples

respectively, in the N-methyl-2-pyrrolidone (NMP) solvent to form a slurry. Then the slurry was coated onto the Al foil, followed by drying in vacuum oven at 110 °C for 12 h and then cut into a circular disc with $d = 12$ mm. The 2032 coin-type cells (20 mm in diameter and 32 mm in thickness) were assembled in a glove box under a high purity argon atmosphere. The cells were composed of the prepared cathode, lithium metal as the anode, and a micro porous membrane (Celgard 2300) as a separator and 1 M LiPF6 dissolved in EC/DMC at mass ratio of 1:1 as the electrolyte. The Land battery tester (LAND CT2001A, Wuhan, China) was used to measure the electrochemical properties of samples in the voltage of from 2.0 to 4.8 V at different current densities (1C = 250 mA g^{-1}). Besides, the electrochemical impedance spectra (EIS) of samples were measured by the CHI660D electrochemical workstation with the frequency range from 100 kHz to 0.01 Hz and a perturbation ac voltage signal of 5 mV.

3 Results and discussion

Figure 2 shows the X-ray diffraction patterns of $Li[Li_{0.2}Mn_{0.54}Ni_{0.13}Co_{0.13}]O_2$ samples before and after ZrF_4 coating. All samples are mostly identified as the typical XRD patterns of $LiMO_2$ phase with the hexagonal α-$NaFeO_2$ structure and the space group R-3m. The weak super lattice peaks between 20° and 25° are related to the Li_2MnO_3 phase, belonging to the monocline unit cell C2/m [20, 21]. All the diffraction peaks of cathodes after the ZrF_4 surface modification are similar to the pristine one and no peaks corresponding to the ZrF_4 have been detected owing to the poor crystallinity or low coating amount of ZrF_4. Besides, it can be

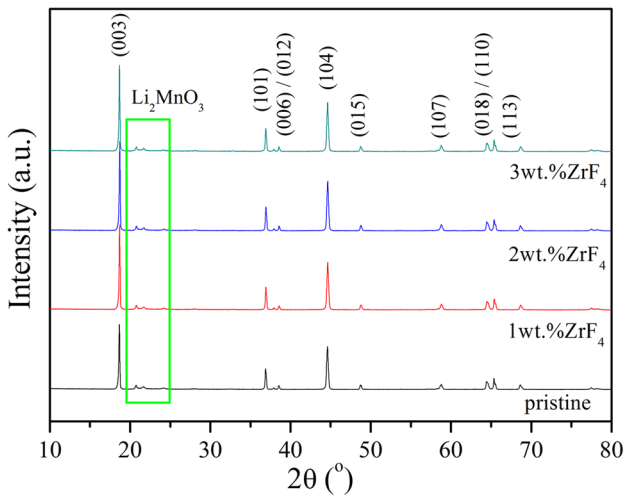

Fig. 2 X-ray diffraction patterns of $Li[Li_{0.2}Mn_{0.54}Ni_{0.13}Co_{0.13}]O_2$ samples before and after ZrF_4 coating

observed that the adjacent peaks of (006)/(102) and (018)/(110) for the four samples have separated obviously, indicating the well hexagonal layered structure of cathode materials have been formed [22]. Table 1 demonstrates the lattice parameters and *c*/*a* values of $Li[Li_{0.2}Mn_{0.54}Ni_{0.13}Co_{0.13}]O_2$ samples before and after ZrF_4 coating, calculated by the XRD software JADE. In the table, the value of *c*/*a* and $I_{(003)}/I_{(104)}$ ratio are the significant indication of cation mixing between Li^+ and Ni^{2+} for the similar ion radii [23, 24]. Partial cation mixing is said to occur if the value of *c*/*a* falls below 4.96 and $I_{(003)}/I_{(104)}$ ration is less than 1.2 [25]. It can be observed that all samples show a high value of *c*/*a* (higher than 4.9900) and $I_{(003)}/I_{(104)}$ peak ratio (larger than 1.50), meaning the $Li[Li_{0.2}Mn_{0.54}Ni_{0.13}Co_{0.13}]O_2$ samples before and after ZrF_4 coating have all demonstrated the low cation-mixing degree.

Figure 3 shows the SEM images of $Li[Li_{0.2}Mn_{0.54}Ni_{0.13}Co_{0.13}]O_2$ samples before and after ZrF_4 coating. All samples appear the similar spherical secondary particles in the size range of 2–7 μm, comprised of the numerous smaller primary particles. Compared with the Fig. 3a, the Fig. 3b–d shows the $Li[Li_{0.2}Mn_{0.54}Ni_{0.13}Co_{0.13}]O_2$ particles after ZrF_4 coating and when the ZrF_4 coating content increases, the surface of the cathode particles present more rough, which may belong to the ZrF_4 nanoparticles and then adhere to the bulk of $Li[Li_{0.2}Mn_{0.54}Ni_{0.13}Co_{0.13}]O_2$.. In order to analyze the surface adhesive materials of the ZrF_4-coated $Li[Li_{0.2}Mn_{0.54}Ni_{0.13}Co_{0.13}]O_2$, the TEM images of pristine $Li[Li_{0.2}Mn_{0.54}Ni_{0.13}Co_{0.13}]O_2$ and 2wt% ZrF_4-coated $Li[Li_{0.2}Mn_{0.54}Ni_{0.13}Co_{0.13}]O_2$ samples have been performed. Compared to the smooth edge lines of pristine $Li[Li_{0.2}Mn_{0.54}Ni_{0.13}Co_{0.13}]O_2$ particles in Fig. 4a, the 2 wt% ZrF_4-coated $Li[Li_{0.2}Mn_{0.54}Ni_{0.13}Co_{0.13}]O_2$ particles in Fig. 4b show an additional coating layer with a thickness from 20 to 40 nm on the surface of the bulk. In addition, combined with the EDS spectra of 2 wt% ZrF_4-coated $Li_{1.2}Mn_{0.54}Ni_{0.13}Co_{0.13}O_2$ sample in Fig. 4d, the detection of Zr and F elements have testified the additional coating layer is the part of ZrF_4 nanoparticles. Figure 4c shows the HR-TEM image of 2 wt% ZrF_4-coated $Li[Li_{0.2}Mn_{0.54}Ni_{0.13}Co_{0.13}]O_2$ sample. The distinct lattice fringes observed in the $Li[Li_{0.2}Mn_{0.54}Ni_{0.13}Co_{0.13}]O_2$ bulk and no lattice fringes detected in the ZrF_4 coating layer have

Table 1 The lattice parameters and *c*/*a* values of the $Li[Li_{0.2}Mn_{0.54}Ni_{0.13}Co_{0.13}]O_2$ samples before and after ZrF_4 coating

Sample	*a* (Å)	*c* (Å)	*c*/*a*	$I_{(003)}/I_{(104)}$
Pristine	2.8472	14.2116	4.9914	1.56
1 wt% ZrF_4	2.8503	14.2305	4.9926	1.63
2 wt% ZrF_4	2.8512	14.2397	4.9943	1.68
3 wt% ZrF_4	2.8529	14.2425	4.9923	1.65

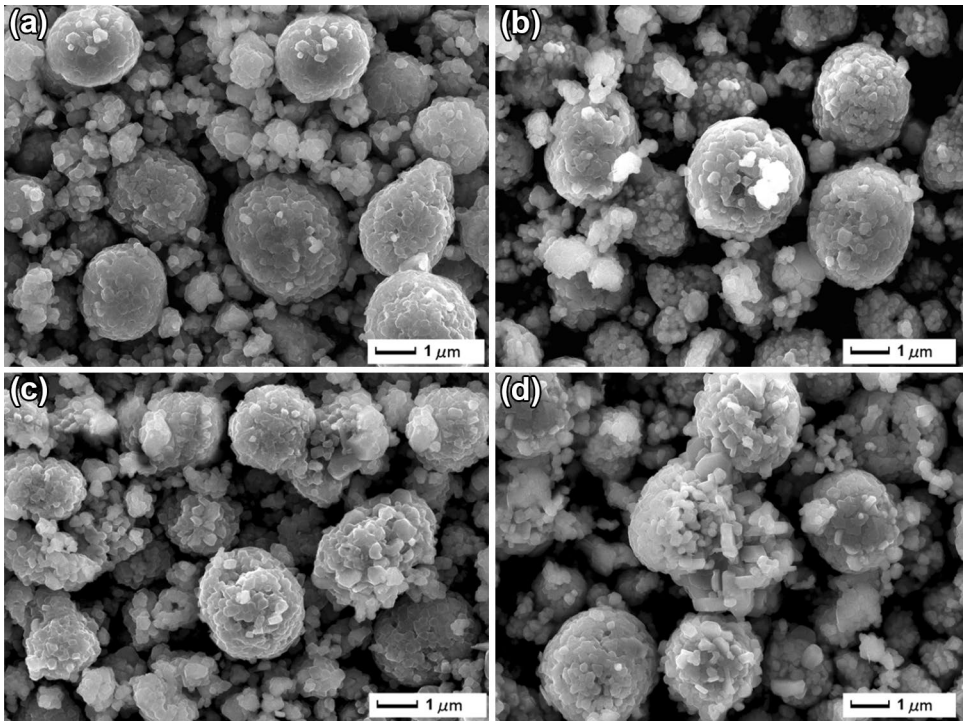

Fig. 3 SEM images of $Li[Li_{0.2}Mn_{0.54}Ni_{0.13}Co_{0.13}]O_2$ samples before and after ZrF_4 coating

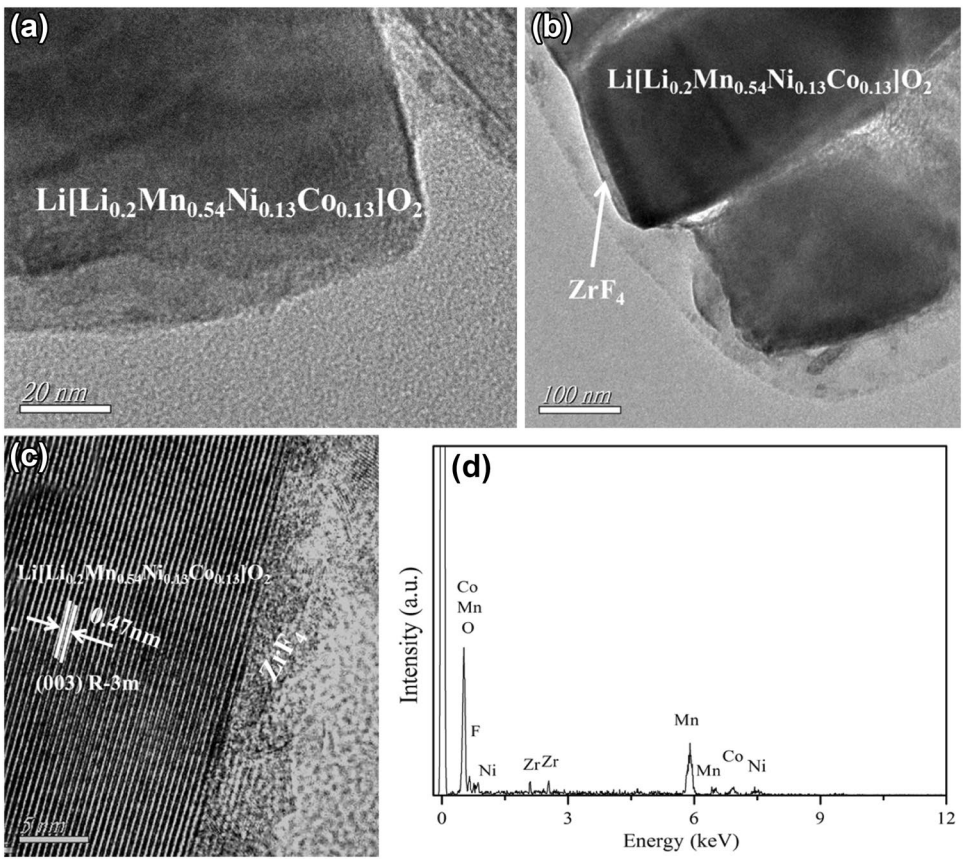

Fig. 4 TEM image of pristine $Li[Li_{0.2}Mn_{0.54}Ni_{0.13}Co_{0.13}]O_2$ (**a**); 2 wt% ZrF_4-coated $Li[Li_{0.2}Mn_{0.54}Ni_{0.13}Co_{0.13}]O_2$ (**b**); HRTEM image of 2 wt%ZrF_4-coated $Li[Li_{0.2}Mn_{0.54}Ni_{0.13}Co_{0.13}]O_2$ (**c**); EDS spectra of 2 wt% ZrF_4-coated $Li[Li_{0.2}Mn_{0.54}Ni_{0.13}Co_{0.13}]O_2$ (**d**)

indicated the $Li[Li_{0.2}Mn_{0.54}Ni_{0.13}Co_{0.13}]O_2$ particles are covered by the amorphous ZrF_4 films.

Figure 5 shows the initial charge and discharge profiles of $Li[Li_{0.2}Mn_{0.54}Ni_{0.13}Co_{0.13}]O_2$ samples before and after ZrF_4 coating between 2.0 and 4.8 V at 0.1C rate. All samples demonstrate the two typical charge areas during the initial charge process, i.e., an initial sloping voltage region and a plateau voltage at 4.5V. The sloping voltage region is relate to the oxidation of Ni^{2+} to Ni^{4+} and Co^{3+} to Co^{4+}, corresponding to the Li^+-extraction from $LiMO_2$ component [26]. While the plateau voltage at 4.5 V is connected with the activation of the Li_2MnO_3 phase, where the Li^+ ion extract and lattice O release (as Li_2O) from the Li_2MnO_3 component irreversibly, causing a large irreversible capacity loss [27]. Table 2 shows the initial charge–discharge data of $Li[Li_{0.2}Mn_{0.54}Ni_{0.13}Co_{0.13}]O_2$ samples before and after ZrF_4 coating between 2.0 and 4.8 V at 0.1 C rate. With the ZrF_4 coating content increasing, the initial discharge capacity increases first and then decreases, and the discharge specific capacities of the four samples are 254.7, 261.2, 271.3 and 267.5 mAh g^{-1}, respectively. In addition, the lower irreversible capacity loss for the ZrF_4-coated $Li[Li_{0.2}Mn_{0.54}Ni_{0.13}Co_{0.13}]O_2$ samples have promoted the higher initial coulombic efficiency. The initial coulombic efficiency are 74.6, 78.8 and 75.3% for ZrF_4-doped $Li[Li_{0.2}Mn_{0.54}Ni_{0.13}Co_{0.13}]O_2$ samples with 1, 2 and 3 wt% coating contents, larger than that (72.1%) of the pristine $Li[Li_{0.2}Mn_{0.54}Ni_{0.13}Co_{0.13}]O_2$. It suggests that the ZrF_4 coating layer can restrain the release of oxygen from the Li_2MnO_3 and decrease the irreversible capacity loss. The reason is that the substitution of F^- for $O^{2-}$from the ZrF_4 coating layer alters the electronic environment and restrains the mobility or release of O^{2-} from Li_2MnO_3 phase [28].

Figure 6 shows the cycling performance of $Li[Li_{0.2}Mn_{0.54}Ni_{0.13}Co_{0.13}]O_2$ samples before and after ZrF_4 coating at 0.5 C rate between 2.0 and 4.8 V for 100 cycles. The plots demonstrate that the samples after ZrF_4 coating distinctly deliver the improved cycling performance in comparison with the pristine $Li[Li_{0.2}Mn_{0.54}Ni_{0.13}Co_{0.13}]O_2$. Among the four samples, the 2wt% ZrF_4-coated $Li[Li_{0.2}Mn_{0.54}Ni_{0.13}Co_{0.13}]O_2$ cathode exhibits the optimal cycling stability. With the ZrF_4 coating content increasing, the initial discharge capacities of the $Li[Li_{0.2}Mn_{0.54}Ni_{0.13}Co_{0.13}]O_2$ samples before and after ZrF_4 coating are 195.0, 204.5, 212.6 and 207.0 mAh g^{-1} respectively. After 100 cycles, the ZrF_4-coated $Li[Li_{0.2}Mn_{0.54}Ni_{0.13}Co_{0.13}]O_2$ samples exhibit the discharge capacity of 180.3, 195.4 and 185.4 mAh g^{-1} with the 1, 2 and 3 wt% coating contents, corresponding that the capacity

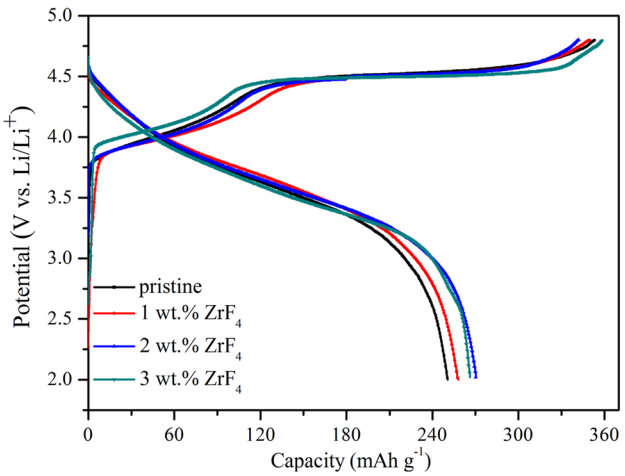

Fig. 5 Initial charge and discharge profiles of $Li[Li_{0.2}Mn_{0.54}Ni_{0.13}Co_{0.13}]O_2$ samples before and after ZrF_4 coating between 2.0 and 4.8 V at 0.1 C rate

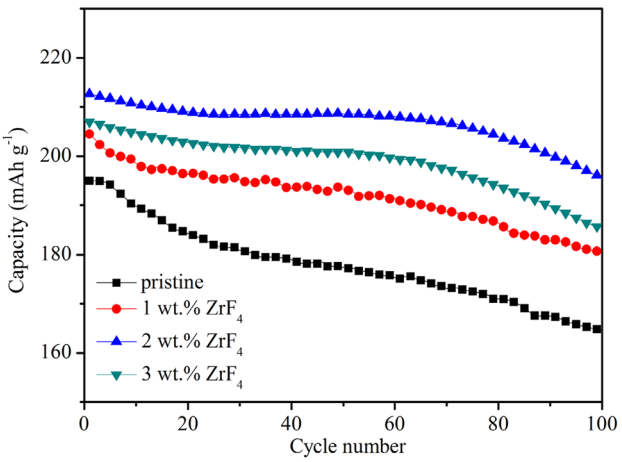

Fig. 6 Cycling performance of $Li[Li_{0.2}Mn_{0.54}Ni_{0.13}Co_{0.13}]O_2$ samples before and after ZrF_4 coating at 0.5 C rate between 2.0 and 4.8 V for 100 cycles

Table 2 Initial charge–discharge data of $Li[Li_{0.2}Mn_{0.54}Ni_{0.13}Co_{0.13}]O_2$ samples before and after ZrF_4 coating between 2.0 and 4.8 V at 0.1 C rate

Samples	Specific charge capacity (mAh g^{-1})	Specific discharge capacity (mAh g^{-1})	Irreversible capacity loss (mAh g^{-1})	Coulombic efficiency (%)
Pristine	353.5	254.7	98.8	72.1
1 wt% ZrF_4	350.1	261.2	88.9	74.6
2 wt% ZrF_4	344.3	271.3	73.0	78.8
3 wt% ZrF_4	355.1	267.5	87.6	75.3

retentions first enhance from 88.2 to 91.9% and then decline to 89.6%. As for the pristine $Li[Li_{0.2}Mn_{0.54}Ni_{0.13}Co_{0.13}]O_2$, the discharge capacity decreases acutely to 164.7 mAh g^{-1} with the capacity retention of only 84.5%. Besides, the data in Fig. 6 has been fitted by linear function, the corresponding relationship equations between discharge capacity (C) and cycle number (N) can be listed as follows:

$$C = 191.1 - 0.27\,N \text{ (pristine cathode)} \quad (1)$$

$$C = 201.6 - 0.20\,N \left(1wt\%\, ZrF_4 - \text{coated cathode}\right) \quad (2)$$

$$C = 212.8 - 0.12\,N \left(2wt\%\, ZrF_4 - \text{coated cathode}\right) \quad (3)$$

$$C = 207.7 - 0.18\,N \left(3wt\%\, ZrF_4 - \text{coated cathode}\right) \quad (4)$$

The corresponding relationship equations (1)-(4) have obviously suggested that the ZrF_4-coated $Li[Li_{0.2}Mn_{0.54}Ni_{0.13}Co_{0.13}]O_2$ samples deliver the higher inherent discharge capacities and the lower decrease slope of discharge capacity with cycle number in comparison with the pristine $Li[Li_{0.2}Mn_{0.54}Ni_{0.13}Co_{0.13}]O_2$ cathode. The superior cycling performance for the ZrF_4-coated samples can be ascribed to the existence of the ZrF_4 coating layer. The ZrF_4 layer can restrict the side reaction between cathodes with electrolyte and protect the cathode surface from further HF corrosion, which contribute to improving the cycling stability during the charge and discharge process.

Figure 7 shows the discharge profiles of $Li[Li_{0.2}Mn_{0.54}Ni_{0.13}Co_{0.13}]O_2$ samples before and after ZrF_4 coating in the 1st, 30th, 60th and 100th cycles at 0.5C rate. It can be seen that, with the cycle going on, the discharge voltage will continuously drop to lower plateaus for all samples owing to the phase transform from the layer structure to spinel-like phase for cathode materials [29]. The high working voltage will aggravate the side reactions between the cathodes with electrolyte, and the dissolution of Mn ions. The dissolution of Mn ions will seriously destroy the cathode layer structure and form the spinel-like phase [30]. The structure damage leads to the attenuation of discharge capacity and the decline of output voltage. In the end, the energy output of the cells will be insufficient to meet the demand of the electronic products, especially in EV and HEV. Table 3 shows the difference value of discharge mid-point voltage (ΔV) between 1st and 100th cycle

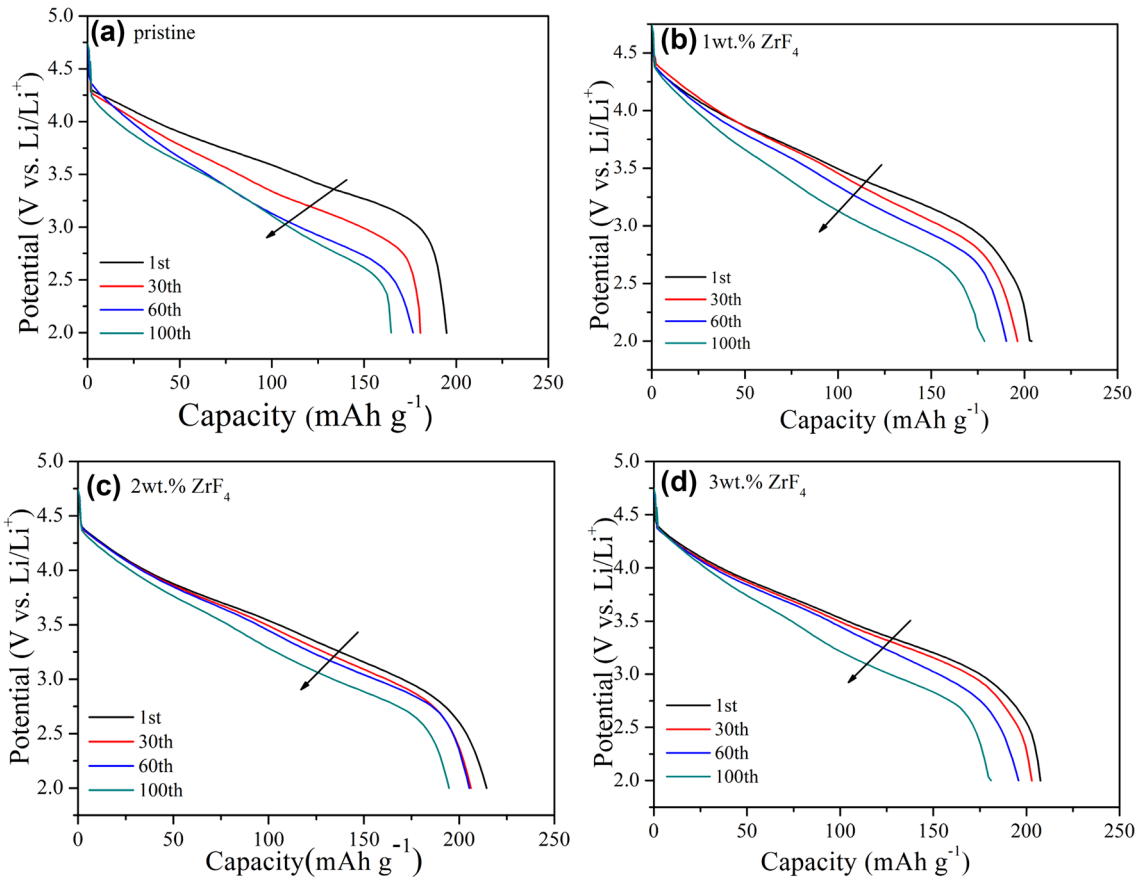

Fig. 7 Discharge profiles of $Li[Li_{0.2}Mn_{0.54}Ni_{0.13}Co_{0.13}]O_2$ samples before and after ZrF_4 coating in the 1st, 30th, 60th and 100th cycles at 0.5 C rate

Table 3 Discharge capacity and the difference value of discharge mid-point voltage (ΔV) for $Li[Li_{0.2}Mn_{0.54}Ni_{0.13}Co_{0.13}]O_2$ samples before and after ZrF_4 coating at 0.5 C rate between 2.0 and 4.8 V

Sample	Initial discharge specific capacity (mAh g^{-1})	100th specific discharge capacity (mAh g^{-1})	100 cycles capacity retention (%)	Declining value of voltage plateau (ΔV) (V)
Pristine	195.0	164.7	84.5	0.34
1 wt% ZrF_4	204.5	180.3	88.2	0.29
2 wt% ZrF_4	212.6	195.4	91.9	0.22
3 wt% ZrF_4	207.0	185.4	89.6	0.25

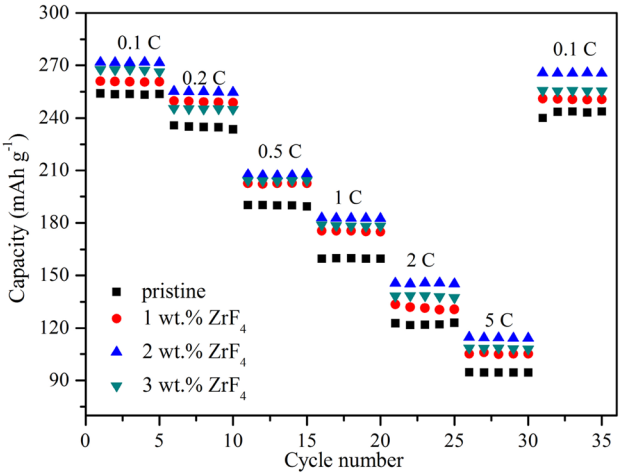

Fig. 8 Rate capability of $Li[Li_{0.2}Mn_{0.54}Ni_{0.13}Co_{0.13}]O_2$ samples before and after ZrF_4 coating at rates of 0.1, 0.2, 0.5, 1, 2, 5 and 0.1 C in sequence for each 5 cycles between 2.0 and 4.8 V

collected by the Land battery tester. The difference value of discharge mid-point voltage are 0.29, 0.22 and 0.25 V for ZrF_4-coated $Li[Li_{0.2}Mn_{0.54}Ni_{0.13}Co_{0.13}]O_2$ samples with 1, 2 and 3 wt% coating contents, respectively, smaller than that (0.34V) of the pristine $Li[Li_{0.2}Mn_{0.54}Ni_{0.13}Co_{0.13}]O_2$. It is obvious that the ZrF_4-coated samples can maintain the high working output voltage in comparison with the pristine $Li[Li_{0.2}Mn_{0.54}Ni_{0.13}Co_{0.13}]O_2$ during cycling. This result indicates that the ZrF_4 coating layer can enhance the layered structure stability by restraining the side reactions between the cathodes with electrolyte and the dissolution of Mn ions.

Rate capability is another important parameter to evaluate the performance of lithium-ion battery. Figure 8 shows the discharge capacities of $Li[Li_{0.2}Mn_{0.54}Ni_{0.13}Co_{0.13}]O_2$ samples before and after ZrF_4 coating at rates of 0.1, 0.2, 0.5, 1, 2, 5 and 0.1 C in sequence for each 5 cycles between 2.0 and 4.8 V. The discharge capacities gradually decrease with the increasing of current density. Compared to the pristine $Li[Li_{0.2}Mn_{0.54}Ni_{0.13}Co_{0.13}]O_2$, the ZrF_4 coated cathodes have obviously exhibited the superior rate capacity. And among the four samples, the 2wt% ZrF_4-coated $Li[Li_{0.2}Mn_{0.54}Ni_{0.13}Co_{0.13}]O_2$ sample demonstrates the optimal rate capability. As is seen in Table 4, the discharge capacities of 2 wt% ZrF_4-coated $Li[Li_{0.2}Mn_{0.54}Ni_{0.13}Co_{0.13}]O_2$ are 271.8, 255.1, 207.5, 182.8, 145.6 and 114.7 mAh g^{-1} at the current density of 0.1, 0.2, 0.5, 1, 2, 5 C rate, respectively. While the pristine electrode exhibits discharge capacity of 254.0, 235.8, 190.2, 159.6, 122.8 and 94.6 mAh g^{-1} at the correspondingly increased current density. It is obvious that the discharge capacity of 2 wt% ZrF_4-coated $Li[Li_{0.2}Mn_{0.54}Ni_{0.13}Co_{0.13}]O_2$ is approximately 20.0 mAh g^{-1} larger than that of the pristine $Li[Li_{0.2}Mn_{0.54}Ni_{0.13}Co_{0.13}]O_2$ at various current densities. The superior rate capacity of the ZrF_4-coated $Li[Li_{0.2}Mn_{0.54}Ni_{0.13}Co_{0.13}]O_2$ samples have mainly been attributed to the fast Li^+ migration speed during the charge and discharge process. Table 1 have demonstrated that the lattice parameters *c* and *a* of the ZrF_4-coated $Li[Li_{0.2}Mn_{0.54}Ni_{0.13}Co_{0.13}]O_2$ samples are larger than those of the pristine $Li[Li_{0.2}Mn_{0.54}Ni_{0.13}Co_{0.13}]O_2$. It indicates the diffusion path of Li^+ insertion/extraction will be expanded and the Li^+ diffusion resistance will decrease during the charge and discharge process after the ZrF_4 coating. In addition, when the current rate is back to 0.1 C, a high discharge capacity of 265.8 mAh g^{-1} is obtained for the 2 wt% ZrF_4-coated $Li[Li_{0.2}Mn_{0.54}Ni_{0.13}Co_{0.13}]O_2$, with about 97.8% discharge capacity left compared to that of the initial cycle at the same rate. While, the pristine electrode only exhibits the capacity retention of 94.5% contrasted with the initial cycle.

Table 4 Discharge capacity of $Li[Li_{0.2}Mn_{0.54}Ni_{0.13}Co_{0.13}]O_2$ samples before and after ZrF_4 coating at various current densities in the voltage range of 2.0-4.8 V

Sample	0.1 C rate (mAh g^{-1})	0.2 C rate (mAh g^{-1})	0.5 C rate (mAh g^{-1})	1 C rate (mAh g^{-1})	2 C rate (mAh g^{-1})	5 C rate (mAh g^{-1})	Follow-up 0.1 C rate (mAh g^{-1})
Pristine	254.0	235.8	190.2	159.6	122.8	94.6	240.0
1 wt% ZrF_4	261.0	249.7	202.6	175.4	133.5	105.3	251.1
2 wt% ZrF_4	271.8	255.1	207.5	182.8	145.6	114.7	265.8
3 wt% ZrF_4	267.7	245.5	204.4	178.8	138.4	108.6	255.7

This result indicates that the ZrF_4 coating layer contributes to the reversibility of Li^+ intercalation and deintercalation across the cathode.

To investigate the influence of ZrF_4 coating layer on the kinetics of Li^+ insertion/extraction into $Li[Li_{0.2}Mn_{0.54}Ni_{0.13}Co_{0.13}]O_2$, the electrochemical impedance spectroscopy (EIS) of the four samples have been performed at a charge state of 4.5 V in different cycles. Figure 9 shows the Nyquist plots of the as-prepared electrodes, and all the Nyquist plots present the same characteristics, including a small semicircle in the high frequency, a large semicircle in the high to medium frequency and a quasi-straight line in the low frequency [31]. The small semicircle in the high frequency corresponds to the impedance of Li^+ migration across the SEI film (R_{sf} *and* CPE_{sf}). The large semicircle in the high to medium frequency is related with the impedance of charge transfer (R_{ct} *and* CPE_{dl}). And the quasi-straight line in the low frequency is connected with the impedance of Li-ion migration in the cathode (Z_W) [32, 33]. The corresponding equivalent circuit in Fig. 9e is used to give a quantitative result, which is simulated by the Zsimpwin software and demonstrated in Table 5. In the 1st cycle, the ZrF_4-coated $Li[Li_{0.2}Mn_{0.54}Ni_{0.13}Co_{0.13}]O_2$ electrode exhibits the lower values of R_s, R_{sf}, R_{ct} than those of pristine one, therefore, the superior initial discharge capacities have been obtained for the ZrF_4 surface modification samples compared to the pristine sample. During the charge and discharge process, the side reaction between the cathode and electrolyte can generate some by-product, which will deposit at the electrode/electrolyte interface to form the Solid Electrolyte Interface (SEI) film, resulting in the increasing values

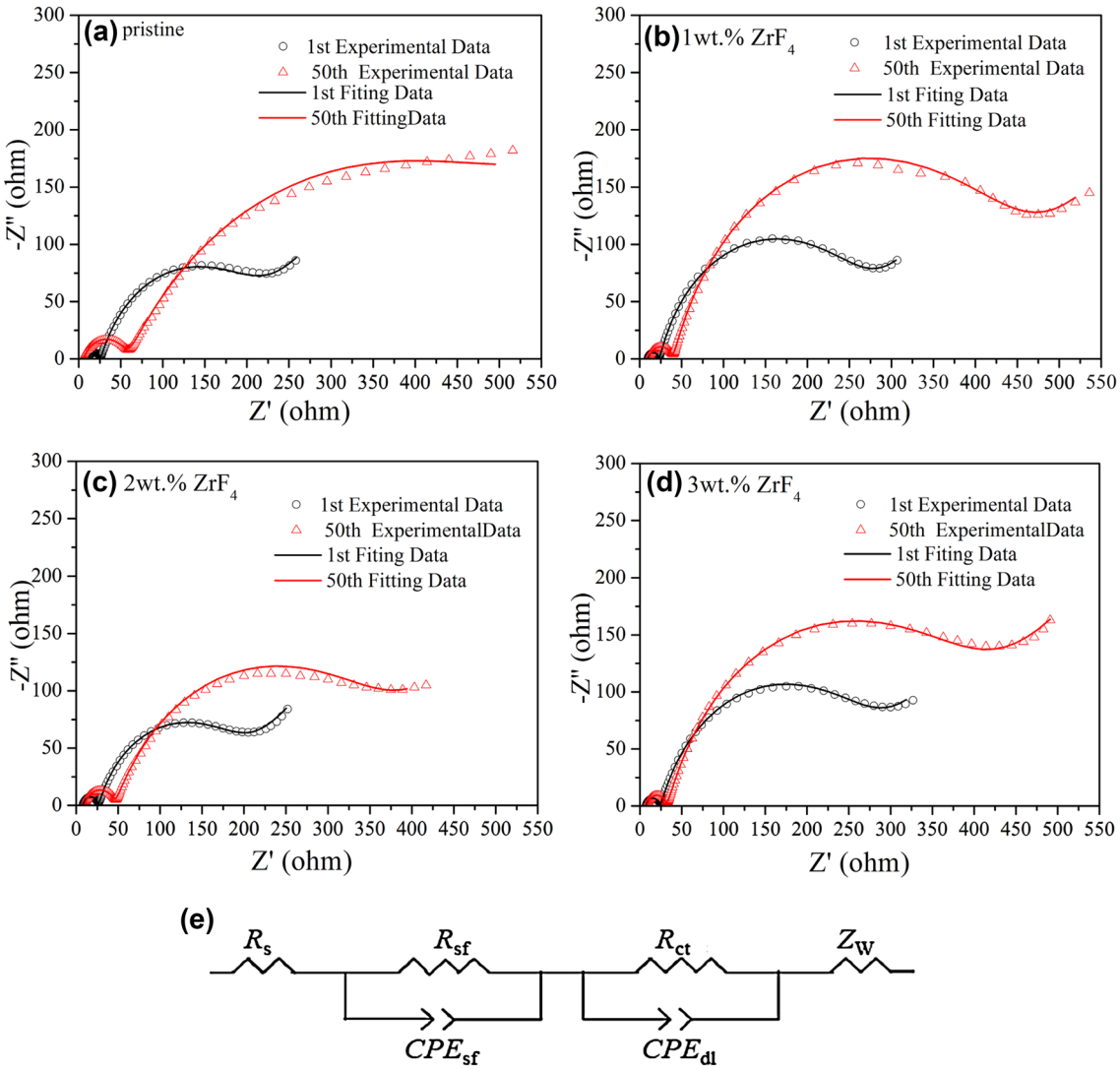

Fig. 9 **a–d** Nyquist plots of $Li[Li_{0.2}Mn_{0.54}Ni_{0.13}Co_{0.13}]O_2$ samples before and after ZrF_4 coating at a charge state of 4.5 V in the 1st and 50th cycle and **e** the equivalent circuit used to fit the measured impedance spectra

Table 5 Fitting data of the Nyquist plot at different cycles of $Li[Li_{0.2}Mn_{0.54}Ni_{0.13}Co_{0.13}]O_2$ samples before and after ZrF_4 coating

Sample	Cycle number	R_s (Ω)	R_{sf} (Ω)	R_{ct}(Ω)	ΔR_{sf}(Ω)
Pristine	1st	5.6	175.1	24.62	459.4
	50th	10.5	634.5	73.44	
1 wt% ZrF_4	1st	5.2	169.3	24.05	365.7
	50th	8.9	535.0	68.33	
2 wt% ZrF_4	1st	4.0	159.3	20.91	255.8
	50th	7.6	415.1	45.87	
3 wt% ZrF_4	1st	5.1	165.3	23.92	311.1
	50th	8.3	476.4	55.83	

of R_{sf} during the charge and discharge process. After 50 cycles, the ZrF_4-coated $Li[Li_{0.2}Mn_{0.54}Ni_{0.13}Co_{0.13}]O_2$ samples exhibit the ΔR_{sf} values of 365.7, 255.8 and 311.1 Ω with 1, 2 and 3 wt% coating contents, respectively, much lower than that (459.4Ω) of the pristine electrode, implying that the weak side reactions between the cathode and electrolyte have occurred for the ZrF_4-coated $Li[Li_{0.2}Mn_{0.54}Ni_{0.13}Co_{0.13}]O_2$ electrodes owing to the existence of ZrF_4 coating layer. Besides, the Li^+ diffusion rate in the cathode can be calculated through the relationship with the impedance of Li-ion migration in the cathode (Z_W), demonstrated as the quasi-straight line in the low frequency of EIS [34]. The corresponding relationship equations are listed as follows:

$$D_{Li^+} = \frac{0.5R^2T^2}{F^4n^4A^2C^2\tau_W} \tag{5}$$

where R, *T, F, n, A, C* are the gas constant, the absolute temperature, the Faraday constant, the number of electrons per molecule during oxidation, the area of the electrode–electrolyte interface, and the concentration of lithium ion, respectively. Besides, τ_W is the Warburg coefficient of the bulk cathode, which is can be calculated by using the following equation:

$$Z_W = S + \tau_W\omega^{-1/2} \tag{6}$$

where *S*, ω are a constant and the angular frequency. And the value of Z_W has been simulated by the Zsimpwin software. According to Eqs. (5) and (6), after 50 cycles, the ZrF_4-coated $Li[Li_{0.2}Mn_{0.54}Ni_{0.13}Co_{0.13}]O_2$ samples exhibit the D_{Li+} values of 4.6×10^{-14} cm^2 s^{-1}, 9.3×10^{-14} cm^2 s^{-1} and 6.4×10^{-14} cm^2 s^{-1} with 1, 2 and 3 wt% coating contents, respectively, higher than that (8.6×10^{-15} cm^2 s^{-1}) of the pristine electrode. Therefore, the better rete capacity of ZrF_4-coated $Li[Li_{0.2}Mn_{0.54}Ni_{0.13}Co_{0.13}]O_2$ samples have been acquired. The weak side reactions between the cathode and electrolyte and the fast Li^+ diffusion coefficient in the cathode for the samples after ZrF_4 coating have effectively contributed to improving the electrochemical properties.

Figure 10 shows the XPS spectra of the pristine and 2 wt% ZrF4-coated $Li[Li_{0.2}Mn_{0.54}Ni_{0.13}Co_{0.13}]O_2$ samples. All XPS spectra are fitted by using XPSPEAK4.1 software. As is seen in Fig. 10a, the Zr 3d is fitted with two peaks at 182.8 eV and 184.9 eV, which are respectively corresponding to ZrO_2 and ZrF_4 with the unique state of 4^+ [35], indicating the ratio of Zr and F of the coating material is 1:4. As seen in Fig. 10b–d, the XPS spectra show that the binding energies of Mn_{2p}, Co_{2p} and Ni_{2p} peaks for 2 wt% ZrF4-coated $Li[Li_{0.2}Mn_{0.54}Ni_{0.13}Co_{0.13}]O_2$ have no obvious changes in comparison with the pristine $Li[Li_{0.2}Mn_{0.54}Ni_{0.13}Co_{0.13}]O_2$. This implies that the valence state of Mn, Co and Ni ions in the structure is not altered [36]. The above discussion has implied that the chemical properties of the metal elements have not been changed after the ZrF_4 coating modification.

4 Conclusions

In summary, the nanoparticles ZrF_4 layer with different contents have been successfully covered on the Li-excess $Li[Li_{0.2}Mn_{0.54}Ni_{0.13}Co_{0.13}]O_2$ cathode materials by using the carbonate co-precipitation method, followed by the chemical deposition technology. The TEM image of the 2 wt% ZrF_4-coated $Li[Li_{0.2}Mn_{0.54}Ni_{0.13}Co_{0.13}]O_2$ particles have demonstrated the amorphous ZrF_4 layer shows the thickness in the range of 20–40 nm. The comparison of electrochemical properties for the $Li[Li_{0.2}Mn_{0.54}Ni_{0.13}Co_{0.13}]O_2$ samples before and after ZrF_4 coating have indicated the ZrF_4 coating layer is favorable for improving the initial irreversible capacity loss, cycling performance and rate capacity of the $Li[Li_{0.2}Mn_{0.54}Ni_{0.13}Co_{0.13}]O_2$.

Among the four samples, the 2 wt% ZrF_4-coated $Li[Li_{0.2}Mn_{0.54}Ni_{0.13}Co_{0.13}]O_2$ demonstrates the prime electrochemical properties. A high capacity retention of 91.9% (195.4 mAh g^{-1}) after 100 cycles at 0.5 C rate is acquired for the 2 wt% ZrF_4-coated $Li[Li_{0.2}Mn_{0.54}Ni_{0.13}Co_{0.13}]O_2$ owing to the effective suppression of side reaction between cathode and electrolyte by the ZrF_4 coating layer, while the pristine $Li[Li_{0.2}Mn_{0.54}Ni_{0.13}Co_{0.13}]O_2$ only delivers the capacity retention of 84.5%. In addition, the ZrF_4-coated $Li[Li_{0.2}Mn_{0.54}Ni_{0.13}Co_{0.13}]O_2$ cathodes have maintained the high working output voltage in comparison with the pristine $Li[Li_{0.2}Mn_{0.54}Ni_{0.13}Co_{0.13}]O_2$ during cycling for that the ZrF_4 coating layer can enhance the layered structure stability by restraining the dissolution of Mn ions. The higher Li^+ diffusion rate in the cathode for the ZrF_4-coated $Li[Li_{0.2}Mn_{0.54}Ni_{0.13}Co_{0.13}]O_2$ samples has deeply contributed to enhancing the high rate capacity compared to the pristine $Li[Li_{0.2}Mn_{0.54}Ni_{0.13}Co_{0.13}]O_2$.

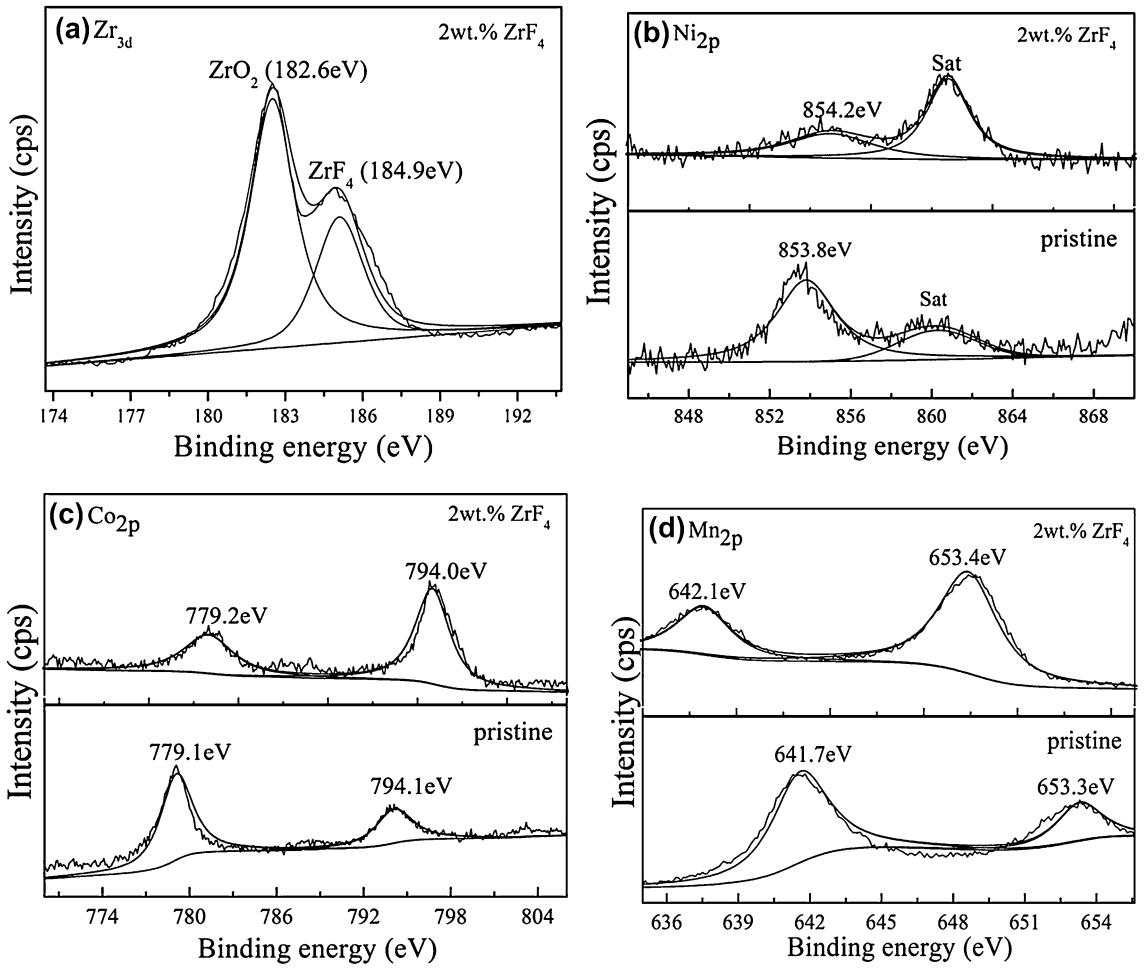

Fig. 10 XPS spectra of the pristine and 2 wt% ZrF4-coated $Li[Li_{0.2}Mn_{0.54}Ni_{0.13}Co_{0.13}]O_2$ samples

Acknowledgements This work was supported by the Natural Science Foundation of Hebei University of Technology (Grant No. 15YCKLQ004).

References

1. M.J. Armstrong, C.O. Dwyer, W.J. Macklin, J.D. Holmes, Evaluating the performances of nanostructured materials as lithium ion battery electrodes. Nano Res. **7**, 1–62 (2014)
2. J. Ou, L. Yang, X.H. Xi, Flour-assisted simple fabrication of $LiCoO_2$ with enhanced electrochemical performances for lithium ion batteries. J. Mater. Sci. **27**, 9008–9014 (2016)
3. Z. Yi, Rheological phase reaction synthesis of Co-doped $LiMn_2O_4$ octahedral particles. J. Mater. Sci. **27**, 10347–10352 (2016)
4. W. Tang, L.L. Liu, S. Tian, L. Li, Y.B. Yue, Y.P. Wu, S.Y. Guan, K. Zhu, Nano-$LiCoO_2$ as cathode material of large capacity and high rate capability for aqueous rechargeable lithium batteries. Electrochem. Commun. **12**, 1524–1526 (2010)
5. F. Wu, J. Tian, Y.F. Su, Y.B. Guan, Y. Jin, Z. Wang, T. He, L.Y. Bao, S. Chen, Lithium-active molybdenum trioxide coated LiNi0.5Co0.2Mn0.3O2 cathode material with enhanced electrochemical properties for lithium-ion batteries. J. Power Sour. **269**, 747–754 (2014)
6. Y.Y. Liu, C.B. Cao, J. Li, Enhanced electrochemical performance of carbon nanospheres–$LiFePO_4$ composite by PEG based sol–gel synthesis. Electrochim. Acta **55**, 3921–3926 (2010)
7. S. Zhao, Y. Bai, Q.J. Chang, Y.Q. Yang, W.F. Zhang, Surface modification of spinel $LiMn_2O_4$ with FeF_3 for lithium ion batteries. Electrochim. Acta **108**, 727–735 (2013)
8. X. Jiang, Z.H. Wang, D. Rooney, X.X. Zhang, J. Feng, J.S. Qiao, W. Sun, K.N. Sun, A design strategy of large grain lithium-rich layered oxides for lithium-ion batteries cathode. Electrochim. Acta **160**, 131–138 (2015)
9. Z. Shen, Dong Li, Influence of lithium content on the structural and electrochemical properties of $Li_{1.20+x}Mn_{0.54}Ni_{0.13}Co_{0.13}O_2$ cathode materials for Li-ion batteries. J. Mater. Sci. (2017). doi:10.1007/s10854-017-7160-7
10. L.J. Xi, C.W. Cao, R.G. Ma, Y. Wang, S.L. Yang, J.Q. Deng, M. Gao, F. Lian, Z.G. Lu, C.Y. Chung, Layered Li2MnO3·3LiNi(0.5-*x*)Mn(0.5-*x*)Co(2*x*)O2 microspheres with Mn-rich cores as high performance cathode materials for lithium ion batteries. Phys. Chem. Chem. Phys. **15**, 16579–16585 (2013)
11. S.J. Shi, J.P. Tu, Y.Y. Tang, Y.X. Yu, Y.Q. Zhang, X.L. Wang, Synthesis and electrochemical performance of

$Li_{1.131}Mn_{0.504}Ni_{0.243}Co_{0.122}O_2$ cathode materials for lithium ion batteries via freeze drying. J. Power Sour. **221**, 300–307 (2013)
12. E.S. Han, Y.P. Li, L.Z. Zhu, L. Zhao, The effect of MgO coating on $Li_{1.17}Mn_{0.48}Ni_{0.23}Co_{0.12}O_2$ cathode material for lithium ion batteries. Solid State Ionics **255**, 113–119 (2014)
13. Q. Xi. Bian, X. Fu, P. Bie, H. Yang, Q. Qiu, G. Pang, F. Chen, Y. Du, Wei, Improved electrochemical performance and thermal stability of Li-excess $Li_{1.18}Co_{0.15}Ni_{0.15}Mn_{0.52}O_2$ cathode material by Li_3PO_4 surface coating. Electrochim. Acta **174**, 875–884 (2015)
14. Z.Y. Wang, E.Z. Liu, C.N. He, C.S. Shi, J.J. Li, N.Q. Zhao, Effect of amorphous $FePO_4$ coating on structure and electrochemical performance of $Li_{1.2}Ni_{0.13}Co_{0.13}Mn_{0.54}O_2$ as cathode material for Li-ion batteries. J. Power Sour. **236**, 25–32 (2013)
15. C. Lu, H. Wu, Y. Zhang, H. Liu, B.J. Chen, N.T. Wu, S. Wang, Cerium fluoride coated layered oxide $Li_{1.2}Mn_{0.54}Ni_{0.13}Co_{0.13}O_2$ as cathode materials with improved electrochemical performance for lithium ion batteries. J. Power Sour. **267**, 682–691 (2014)
16. C. Li, H.P. Zhang, L.J. Fu, H. Liu, Y.P. Wu, E. Rahm, R. Holze, H.Q. Wu, Cathode materials modified by surface coating for lithium ion batteries. Electrochim. Acta **51**, 3872–3883 (2006)
17. G.-H. Lee, I.H. Choi, M.Y. Oh, S.H. Park, K.S. Nahm, V. Aravindan, Y.-S. Lee, Confined ZrO_2 encapsulation over high capacity integrated $0.5Li[Ni_{0.5}Mn_{1.5}]O_4{\cdot}0.5[Li_2MnO_3{\cdot}Li(Mn_{0.5}Ni_{0.5})O_2]$ cathode with enhanced electrochemical performance. Electrochim. Acta **194**, 454–460 (2016)
18. J.Z. Kong, S.S. Wang, G.A. Tai, L. Zhu, L.G. Wang, H.F. Zhai, D. Wu, A.D. Li, H. Li, Enhanced electrochemical performance of $LiNi_{0.5}Co_{0.2}Mn_{0.3}O_2$ cathode material by ultrathin ZrO_2 coating. J. Alloys Compd. **657**, 593–600 (2016)
19. C.-D. Li, Z.-L. Yao, J. Xu, P. Tang, X. Xiong, Surface-modified $Li[Li_{0.2}Mn_{0.54}Ni_{0.13}Co_{0.13}]O_2$ nanoparticles with LaF_3 as cathode for Li-ion battery. Ionics **23**, 549–558 (2017)
20. S. Ma, X. Hou, Y. Li, Q. Ru, S. Hu, K. Lam, Performance and mechanism research of hierarchically structured Li-rich cathode materials for advanced lithium–ion batteries. J. Mater. Sci. **28**, 2705–2715 (2017)
21. F. Wu, Z. Wang, Y. Su, N. Yan, L. Bao, S. Chen, $Li[Li_{0.2}Mn_{0.54}Ni_{0.13}Co_{0.13}]O_2$–$MoO_3$ composite cathodes with low irreversible capacity loss for lithium ion batteries. J. Power Sour. **247**, 20–25 (2014)
22. Q.R. Xue, J.L. Li, G.F. Xu, H.W. Zhou, X.D. Wang, F.Y. Kang, In situ polyaniline modified cathode material $Li[Li_{0.2}Mn_{0.54}Ni_{0.13}Co_{0.13}]O_2$ with high rate capacity for lithium ion batteries. J. Mater. Chem. A **2**, 18613–18623 (2014)
23. L. Li, X. Zhang, R. Chen, T. Zhao, J. Lu, F. Wu, K. Amine, Synthesis and electrochemical performance of cathode material $Li_{1.2}Co_{0.13}Ni_{0.13}Mn_{0.54}O_2$ from spent lithium-ion batteries. J. Power Sour. **249**, 28–34 (2014)
24. M. Bettge, Y. Li, B. Sankaran, N.D. Rago, T. Spila, R.T. Haasch, I. Petrov, D.P. Abrahama, Improving high-capacity $Li_{1.2}Ni_{0.15}Mn_{0.55}Co_{0.1}O_2$-based lithium-ion cells by modifying the positive electrode with alumina. J. Power Sour. **233**, 346–357 (2013)
25. H. Zhang, Q.Q. Qiao, G.R. Li, X.P. Gao, PO_4^{3-} polyanion-doping for stabilizing Li-rich layered oxides as cathode materials for advanced lithium-ion batteries. J. Mater. Chem. A **2**, 7454–7460 (2014)
26. J. Wang, G.X. Yuan, M.H. Zhang, B. Qiu, Y.G. Xia, Z.P. Liu, Li1 +*x*Ni1/6Co1/6Mn4/6O2.25+*x*/2 ($0.1 \leq x \leq 0.7$) cathode materials. Electrochim. Acta **66**, 61–66 (2012)
27. G.B. Liu, H. Liu, Y.F. Shi, The synthesis and electrochemical properties of $x Li_2MnO_3{\cdot}(1\text{-}x)MO_2$ ($M = Mn_{1/3}Ni_{1/3}Fe_{1/3}$) via coprecipitation method. Electrochim. Acta **88**, 112–116 (2013)
28. X.Y. Liu, J.L. Liu, T. Huang, A.S. Yu, CaF_2-coated $Li_{1.2}Mn_{0.54}Ni_{0.13}Co_{0.13}O_2$ as cathode materials for Li-ion batteries. Electrochim. Acta **109**, 52–58 (2013)
29. Y. Li, M. Bettge, B. Polzin, Y. Zhu, M. Balasubramanian, D.P. Abraham, Understanding long-term cycling performance of $Li_{1.2}Ni_{0.15}Mn_{0.55}Co_{0.1}O_2$–graphite lithium-Ion cells. J. Electrochem. Soc. **160**, A3006-A3019 (2013)
30. S.J. Shi, J.P. Tu, Y.J. Zhang, Y.D. Zhang, X.Y. Zhao, X.L. Wang, C.D. Gu, Effect of Sm_2O_3 modification on $Li[Li_{0.2}Mn_{0.56}Ni_{0.16}Co_{0.08}]O_2$ cathode material for lithium ion batteries. Electrochim. Acta **108**, 441–448 (2013)
31. X. Ma, H. He, Y. Sun, Y. Zhang, Synthesis of $Li_{1.2}Mn_{0.54}Co_{0.13}Ni_{0.13}O_2$ by sol-gel method and its electrochemical properties as cathode materials for lithium-ion batteries. J. Mater. Sci. (2017). doi:10.1007/s10854-017-7578-y
32. J.R. Croy, K.G. Gallagher, M. Balasubramanian, Z.H. Chen, Y. Ren, D.H. Kim, S.H. Kang, D.W. Dees, M.M. Thackeray, Examining hysteresis in composite $x Li_2MnO_3{\cdot}(1 - x)LiMO_2$ cathode structures. J. Phys. Chem. C **117**, 6525–6536 (2013)
33. B. Liu, Z. Zhang, J. Wan, S. Liu, Improved electrochemical properties of YF_3-coated $Li_{1.2}Mn_{0.54}Ni_{0.13}Co_{0.13}O_2$ as cathode for Li-ion batteries. Ionics **23**, 1365–1374 (2017)
34. Q. Li, Y. Hu, L. Li, C. Feng, Synthesis and electrochemical performances of Mn*x*Co*y*Ni*z*CO3. J. Mater. Sci. **27**, 1700–1707 (2016)
35. W. Zhu, W. Li, S. Mu, Y. Yang, X. Zuo, The adhesion performance of epoxy coating on AA6063 treated inTi/Zr/V based solution. Appl. Surf. Sci. **384**, 333–340 (2016)
36. J. Zheng, S.N. Deng, Z.C. Shi, H.J. Xu, H. Xu, Y.F. Deng, Z. Zhang, G.H. Chen, The effects of persulfate treatment on the electrochemical properties of $Li[Li_{0.2}Mn_{0.54}Ni_{0.13}Co_{0.13}]O_2$ cathode material. J. Power Sour. **221**, 108–113 (2013)